Traffic 2012; **13:** 705–714

doi:10.1111/j.1600-0854.2012.01339.x

Lipid Droplet *De Novo* Formation and Fission Are Linked to the Cell Cycle in Fission Yeast

Allan P. Long[1], Anna K. Manneschmidt[1], Bobby VerBrugge[1], Mary R. Dortch[1], Steven C. Minkin[2], Keith E. Prater[2], John P. Biggerstaff[2], John R. Dunlap[3] and Paul Dalhaimer[1,4]*

[1]Department of Chemical and Biomolecular Engineering, University of Tennessee, Knoxville, TN 37996, USA
[2]Center for Environmental Biotechnology, University of Tennessee, Knoxville, TN 37996, USA
[3]Advanced Microscopy and Imaging Center, University of Tennessee, Knoxville, TN 37996, USA
[4]Department of Biochemistry and Cellular and Molecular Biology, University of Tennessee, Knoxville, TN 37996, USA

**Corresponding author: Paul Dalhaimer, pdalhaim@utk.edu*

Cells sequester neutral lipids in bodies called lipid droplets. Thus, the formation and breakdown of the droplets are important for cellular metabolism; unfortunately, these processes are difficult to quantify. Here, we used time-lapse confocal microscopy to track the formation, movement and size changes of lipid droplets throughout the cell cycle in fission yeast *Schizosaccharomyces pombe*. In theory, the number of lipid droplets in these cells must increase for daughter cells to have the same number of droplets as the parent at a reference point in the cell cycle. We observed stable droplet formation events in G2 phase that were divided evenly between *de novo* formation of nascent droplets and fission of preexisting droplets. The observations that lipid droplet number is linked to the cell cycle and that droplets can form via fission were both new discoveries. Thus, we scrutinized each fission event for multiple signatures to eliminate possible artifacts from our microscopy. We augmented our time-lapse confocal microscopy with electron microscopy, which showed lipid droplet 'intermediates': droplets shaped like dumbbells that are potentially in transition states between two spherical droplets. Using these complementary microscopy techniques and also dynamic simulations, we show that lipid droplets can form by fission.

Key words: cell cycle, endoplasmic reticulum, fat body, fission yeast, lipid body, lipid droplet, lipid particle

Received 19 August 2011, revised and accepted for publication 31 January 2012, uncorrected manuscript published online 2 February 2012, published online 27 February 2012

The main cellular function of lipid droplets is hypothesized to be the storage of neutral lipids. Lipid droplets consist of a phospholipid monolayer that surrounds a core of neutral lipids, mostly triacylglycerols and sterol esters (1,2). Nascent droplets are hypothesized to form from the endoplasmic reticulum (ER) through singular biogenesis events. The most popular biogenesis model involves the buildup of a 'lens' of neutral lipids in the hydrophobic region of the ER membrane (3–7). The lens grows in size until it becomes spherical – with a diameter on the order of the ER membrane – and separates from the ER, becoming a distinct organelle (3). In other models, the now-spherical droplet remains fixed to the ER in an 'egg cup' geometry (8) or connected to the ER through a tether (4). It is possible that droplets could also be formed by fission of two preexisting droplets, although this has not, to our knowledge, been observed (9,10). The mechanisms, timescales and relative frequencies of formation events have not been determined, although such quantification would lend insight into the ways cells distribute neutral lipids (3,4,9,11–13).

Triggers for droplet formation are still murky. However, the neutral lipid content of cells has recently been linked to cell cycle progression. This is exciting because the role of lipid droplets in cells may be broader than previously believed. The major triacylglycerol lipase (Tgl) in budding yeast, Tgl4p, is phosphorylated and activated by cyclin-dependent kinase 1/cell division cycle protein 28 (Cdk1p/Cdc28p) (14). The resulting lipolysis contributes to bud formation in late G1 phase of the budding yeast cell cycle. Also, lack of lipolysis of triacylglycerols delays the same bud formation. Other earlier work showed that the 4,4-difluoro-1,3,5,7,8-pentamethyl-4-bora-3a,4a-diaza-*s*-indacene (BODIPY 493/503)-stained neutral lipid intensity of MA-10 Leydig tumor cells was a function of the cell cycle, although the cells in that study were cultured in high amounts of oleic acid (15). Neutral lipid biosynthesis has also been reported to be co-ordinated with cell cycle progression in plant cells (16). Thus, there appear to be links between cell cycle progression and neutral lipid turnover, but they are just beginning to be appreciated, and the role of lipid droplets in these processes has yet to be fleshed out.

Here, we used time-lapse confocal microscopy to quantify the formation, dynamics and size changes of individual lipid droplets in the fission yeast *Schizosaccharomyces pombe* during log growth phase. The cells were cultured in yeast extract-based media that was not loaded with fatty acids. Microscopy in one time and three spatial dimensions is necessary to study the formation or breakdown of lipid droplets in yeast (and probably other organisms) because the droplets are dynamic enough that it is impossible to differentiate between creation and annihilation events versus movement in or out of the focal plane using epifluorescence. This is particularly true of

small droplets. Yeast cells are useful for tracking such dynamics because they provide a well-defined volume in which quantitative confocal microscopy can be performed over fast times (17). Fission yeast cells in particular are ideal model systems for studying lipid droplet formation because they have well-defined nuclear and peripheral ERs so that biogenesis from those regions is relatively easy to observe (18).

We show that the number of lipid droplets in fission yeast cells is a function of the cell cycle. There was a consistent increase in the number of lipid droplets during G2 phase. This is where stable *de novo* formation and fission events were observed. Fission of preexisting large lipid droplets seemed to be the main mechanism for producing medium- to large-sized droplets (proportional to their fluorescent intensity) because most small droplets, including those recently formed, did not reach a large size over the same timescales and droplet fusion was not observed.

Results

We used time-lapse confocal microscopy to quantify the dynamics of BODIPY 493/503-stained lipid droplets in a fission yeast *S. pombe* strain with the luminal ER marker mCherry-AHDL integrated into the leu1+ locus (18) (Figure 1A). The use of both markers allowed us to observe potential interactions between the droplets and the ER. BODIPY 493/503 is a lipophilic dye that rapidly partitions into the nonpolar environment of lipid droplets and does not localize appreciably to other cellular structures (19). It also has a relatively narrow emission spectrum, making it ideal for dual localization studies (19). Two independent threshold values were determined for the green and red signals using Otsu's well-established method (20). The calculated thresholds for the BODIPY 493/503 and mCherry-AHDL signals were 7 and 12% of the maximum possible single pixel intensities, respectively. This thresholding eliminated background noise but did not identify the minimum fluorescence that would constitute a lipid droplet. To do so, we performed the following measurements.

Because BODIPY 493/503 partitions into lipid droplets, a larger droplet will be able to accommodate more dye molecules than a smaller droplet. In fact, the fluorescent intensity of a dye-labeled droplet should scale linearly with its volume (21). We measured the fluorescent intensities and diameters of 20 large spherically shaped lipid droplets and fit the relationship between these two measured values with a line (Figure S1). We used the equation of this line to determine the volume (and thus diameter using $V = 4\pi/3*[d/2]^3$) of droplets that were smaller than the resolution of our microscopy using their fluorescent intensity as the independent variable. Small droplets should be spherical because that shape will minimize exposure of the neutral lipids, as the diameter of the droplet approaches the length of the phospholipids that constitute the droplet monolayer (22).

Both the 'lens' and 'bicelle' formation models require that *de novo* droplets have diameters close to the width of the ER membrane: ~5–6 nm (3). We determined the needed fluorescent intensity of a droplet with a diameter of 6 nm from the data in Figure S1. Objects having intensities greater or equal to this value were counted as lipid droplets. In this study, we used the above diameter calculation for the *de novo* formation analysis.

Lipid droplets and the fission yeast cell cycle

Fission yeast cells increase in length by about a factor of two during the cell cycle and subsequently split in half. This implies that the number of lipid droplets must also increase in number at some point during the cycle for each daughter cell to have the same number of lipid droplets as the parent cell did at a reference time-point.

The total number of lipid droplets in fission yeast cells increased during G2 stage of the cell cycle and stayed relatively constant in M, G1 and S phases (Figure 1B,C). We grouped cells in G1 and S phases ('G1/2S') because they are septated the majority of the time, and it is challenging to differentiate between these stages of the cycle as fission yeast do not readily take up bromodeoxyuridine (BrdU), the common marker for S phase (23). Lipid droplets were monitored in all cells in log growth phase in media not loaded with fatty acids. This dependence of lipid droplet number on the cell cycle has not, to our knowledge, been reported up until this point. There was a weaker correlation between the total BODIPY 493/503 fluorescent intensity of the lipid droplets in the cells and the cell cycle (Figure 1D). This implies that the total neutral lipid mass of cells is more stable through the cycle than the number of lipid droplets.

We wished to determine general dynamic properties of lipid droplets. We measured the average fluorescent intensity of each lipid droplet in the cells shown in Figure 1B over 10 min. The distribution of the fluorescence is skewed toward smaller signals, meaning that smaller droplets predominate (Figure 1E). The possible ramifications of this are discussed below. We wished to determine if there were correlations among the size of a droplet, the change in its size and its movement. To do so, we analyzed these three parameters for the droplets in the four cells in Figure 1B over 10 min. Fluctuations in the fluorescent intensity of the droplets over 10 min were inversely related to droplet fluorescence: smaller droplets had larger fluctuations in fluorescence than larger droplets (Figure 1F). This is the opposite of what would be expected as fluctuations should scale with the size of an object affected by thermal energy, such as a lipid droplet (22).

Correlations between root mean square displacement and droplet fluorescent intensity were less clear. Smaller

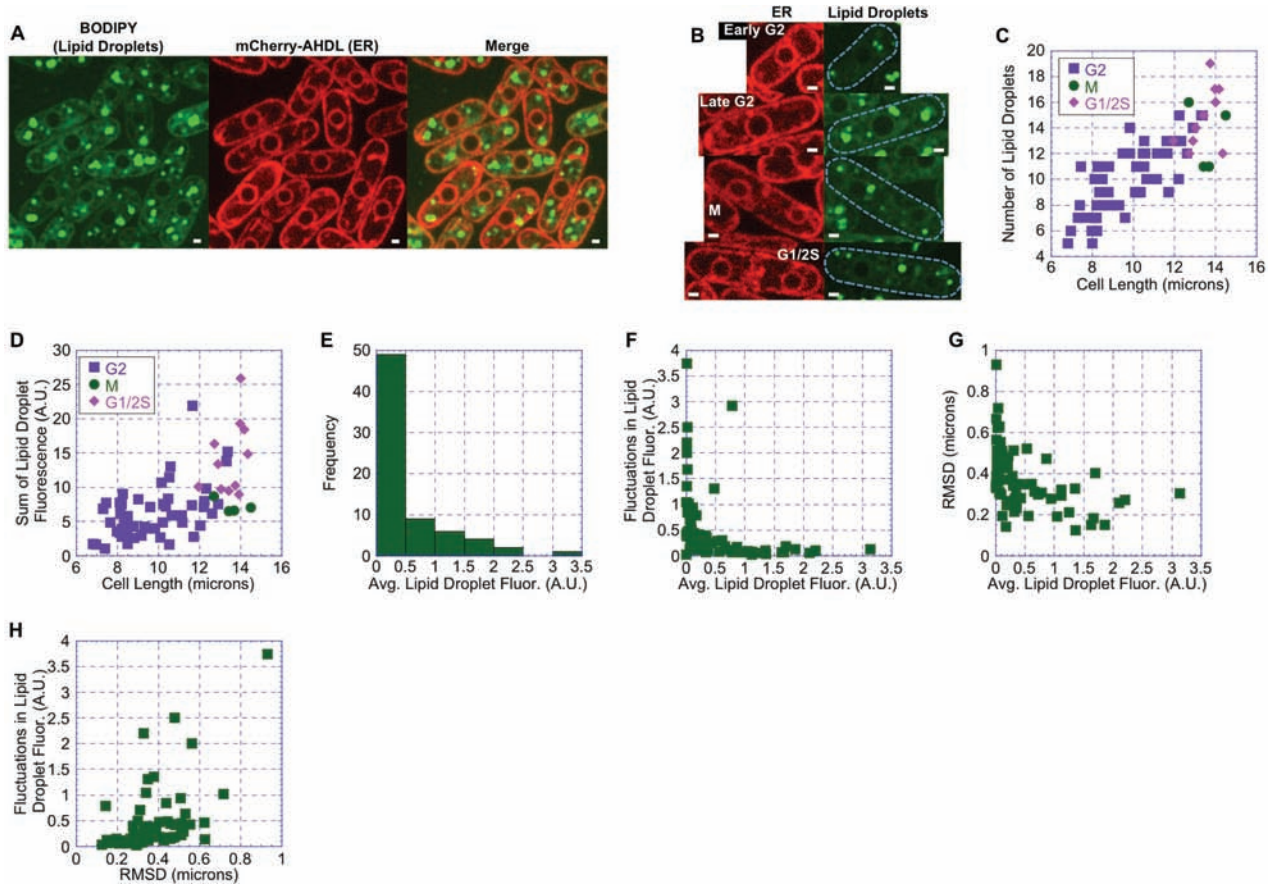

Figure 1: Dynamic properties of lipid droplets in fission yeast cells. A) Single focal plane fluorescent micrographs showing BODIPY 493/503-stained lipid droplets (left), mCherry-AHDL-labeled ER (center) and the merger of the two signals (right) in a group of fission yeast cells. B) Single focal plane fluorescent micrographs showing four different cells in early G2, late G2, M and G1/2S stages of the cell cycle at the nuclear focal plane. Micrographs on the left show the mCherry-AHDL-labeled ER signal and those on the right show the BODIPY 493/503-stained lipid droplets. Dashed outlines represent the exteriors of the cells. C and D) Plots of the number (C) and fluorescent intensity (D) of lipid droplets at a single time-point as a function of cell length and stage of the cell cycle. Data for these plots are from *N* different cells: G2 phase, $n = 56$; M phase, $n = 4$; G1/2S phase, $n = 11$. Linear fit values are $R^2 = 0.7$ for the data in (C) and $R^2 = 0.4$ for the data in (D). E) Distribution of the average fluorescence of the droplets over 10 min in the cells shown in (B). F) Plot of the fluctuations in the fluorescence of each droplet over 10 min versus the average fluorescence of each droplet. G) Plot of the root mean square displacement (RMSD) of each droplet versus the average fluorescence of each droplet over 10 min. H) Plot of the fluctuations in fluorescence of each droplet versus their RMSD. Data for plots (E-H) are from droplets in the cells in (B). Scale bars are 1 μm.

droplets were slightly more mobile than larger ones (Figure 1G). But this should be true of any intracellular object as larger sizes increase steric hindrance with other organelles. However, it is apparent that droplets can have relatively large changes in their fluorescent intensity without being spatially fixed (Figure 1H). Put another way, the droplets are changing sizes while being 'gregarious' (11).

De novo lipid droplet formation

Observing formation events is of keen importance because of the ambiguity in the field over the origins of lipid droplets. We searched for such events in ~75 cells in all stages of the cell cycle by counting the number of droplets at times $t = 0$ and $t = 10$ min using confocal microscopy. If the number of droplets in a cell at $t = 10$ min was greater than the number at $t = 0$ min, we closely examined the cell's three-dimensional (3D) space at 30-second intervals to determine the origin of any nascent droplets. Using this technique, we found 10 total formation events split equally between *de novo* formation and fission in cells in G2 phase.

BODIPY-stained lipid droplets formed *de novo* in cells in G2 phase of the cell cycle (Figure 2 and Movie 1). Again, there are two thresholds that the BODIPY 493/503 signal must overcome for the localized fluorescence to be counted as a lipid droplet: (i) the Otsu threshold (20), which eliminates background fluorescence and (ii) the combined threshold of the pixels above the Otsu threshold that have a strong enough signal to represent a spherical object having a diameter equal to the thickness of the

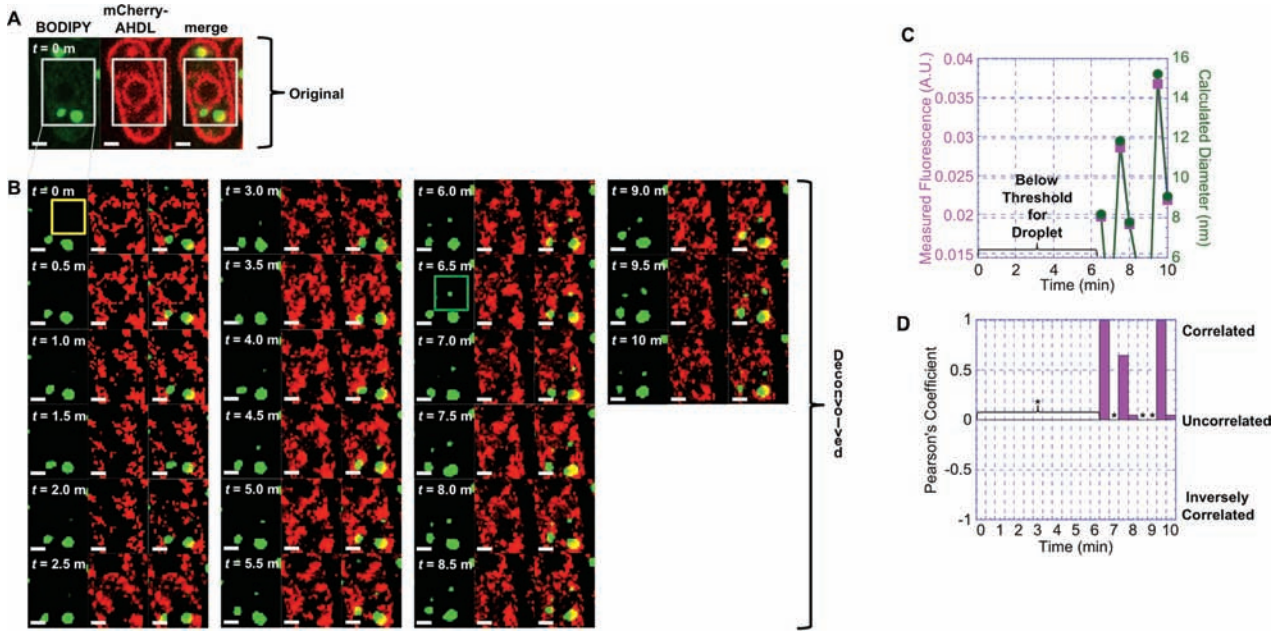

Figure 2: ***De novo*** **lipid droplet formation event in G2 phase of the cell cycle**. A) Original single focal plane fluorescent micrographs showing BODIPY 493/503-stained lipid droplets (left), mCherry-AHDL-labeled ER (center) and the merger of the two signals (right) in a single cell in G2 phase of the cell cycle. B) Projected maximum intensity of the BODIPY 493/503-stained lipid droplets (left), mCherry-AHDL-labeled ER (center) and the merger of the two signals (right) at specified time-points. These images were deconvolved. Yellow rectangle at $t = 0$ min indicates the region where the droplet later appeared. Green rectangle at $t = 6.5$ min shows the location of the fluorescent signal that is first high enough to be counted as a lipid droplet. C) Plot of the measured fluorescent signal (magenta) and calculated diameter (green) of the newly observed droplet. The minimum fluorescent signal corresponds to a droplet diameter that is equal to the thickness of the ER membrane (6 nm). D) Plot of Pearson's colocalization coefficient of the BODIPY 493/503-stained lipid droplets and mCherry-AHDL-labeled ER in the z-stacks where the newly observed droplet was above the minimum threshold in (B). Reported values are maximums of the calculated coefficients in each z-stack. *Time-points where the signal of the droplet was below the minimum as described in the text. Scale bars are 1 μm.

ER membrane, as described above (Figure S1). For one such event, the fluorescent intensity in the 3D volume where the droplet later appeared was below the Otsu threshold before $t = 2.0$ min (Figure 2B). Between $t = 2.0$ and $t = 6.0$ min, the signal rose above the Otsu threshold but was still too low for a fluorescently labeled spherical object to have a diameter greater or equal to 6 nm (Figure 2B). This is not obvious by eye, which is why rigorous quantification of the fluorescent signal is needed. At $t = 6.5$ min, the signal was large enough for the contiguous pixels to be a 6 nm diameter sphere. After $t = 6.5$ min, the signal of the droplet oscillated about this second threshold but with an upward trend (Figure 2B,C). This observed oscillation in fluorescent intensity was common for the five *de novo* formation events. We carried out quantitative colocalization analysis of this lipid droplet and the ER by calculating the maximum value of Pearson's coefficient in the z-stacks in which the newly observed droplet was present (24). The value of Pearson's coefficient can range from 1 to 1, with 1 standing for complete positive correlation, 0 standing for no correlation and 1 for negative correlation. The BODIPY 493/503 and mCherry-AHDL signals were correlated at $t = 6.5$ min, the time-point of formation obtained by our analysis (Figure 2D). The value for Pearson's coefficient fluctuated between correlated and uncorrelated values after this time-point (Figure 2D).

The distance between this newly observed droplet and the closest preexisting droplet was 1.3 μm. If the newly observed droplet would have originated from the closest preexisting droplet, it would have had to travel a distance of 1.3 μm/30 second which is in the top 0.2% of the displacements that we measured for 1400 independent droplet moves. This makes it highly unlikely that this droplet separated from a preexisting droplet.

Lipid droplet fission

Newly observed droplets in G2 phase also originated from preexisting droplets by fission. We define a fission event as the cleaving of a single preexisting lipid droplet, resulting in two independent droplets. Time-lapse confocal microscopy is ideal for capturing such events because the temporal change in shape of the preexisting droplet from a sphere, to an elongated dumbbell-type shape, to two separate spheres can, in theory, be observed. However, the dispersion of *two* preexisting lipid droplets that were *never a single object* may be mistakenly scored as a fission event if the droplets are located too close

to each other to be resolved as distinct entities. In particular, if the preexisting droplet is located at the ER, a new droplet could potentially form *de novo* next to the preexisting droplet at a distance that is less than the spatial resolution of light microscopy. The *de novo* droplet could subsequently move away from the preexisting droplet and possibly appear to be created by fission.

Therefore, several criteria must be met for the appearance of a new droplet to be scored as a fission event: (i) the fluorescent signals of both the preexisting and newly observed droplets cannot be localized to the ER signal until after the droplets have become distinct entities, (ii) the dynamics of the preexisting droplet must reflect the fact that it is a single object before fission was observed and (iii) the size of the newly observed droplet plus the size of the preexisting droplet after fission should closely match the size of the preexisting droplet before fission. In addition, the fluorescent intensity – related to droplet volume as discussed above – of the newly observed droplet should be greater than that possible for a droplet formed *de novo*, although this last condition is not strictly necessary. It should also be noted that fission could still occur at the ER, but it would be difficult to prove such an event.

One of the five fission events is shown in Figure 3 and Movie 2. The original single-plane fluorescent micrographs of the BODIPY 493/503 signal (left), mCherry-AHDL (center) and the merger (right) of the two signals at the widest point of the droplet are shown for the first time-point (Figure 3A). We also show the maximum intensity projections of the deconvolved BODIPY 493/503 and mCherry-AHDL signals from the z-stacks in which the preexisting and newly observed lipid droplets were present (Figure 3B). The preexisting droplet was quasispherical in shape for 8 min, assumed a dumbbell geometry at $t = 8.5$ min and then separated into two stable droplets at $t = 9.5$ min (Figure 3B). The preexisting droplet resided in a gap in the mCherry-AHDL signal (Figure 3B). The maximum-intensity fluorescent signals of BODIPY 493/503 and mCherry-AHDL had no overlap before the observation of fission (Figure 3B). As with the representative *de novo* formation event, we carried out quantitative colocalization analysis of the lipid droplet and the ER by calculating the maximum value of Pearson's coefficient in the z-stacks in which the preexisting droplet and newly observed droplet were present (24). The BODIPY 493/503 and mCherry-AHDL signals did not correlate during this fission event (Figure 3C). This provides strong evidence that the droplet that was first observed as a distinct entity at $t = 9.5$ min in Figure 3B did not originate from the ER.

We wished to determine if the preexisting droplet shown in Figure 3A,B was a single droplet and not two droplets existing at positions next to each other from times $t = 0$ to $t = 9.0$ min that we could not resolve by our microscopy technique. We measured the displacements of ~70 different lipid droplets at 30-second intervals over 10 min (~1400 independent moves) to quantify the general dynamics of the droplets. Ninety percent of the 1400 moves had displacements greater than the baseline of our resolution (133 nm/pixel) over a 30-second time period. Thus, each droplet is highly dynamic on length scales that are quantifiable by confocal microscopy. Also, no two droplets moved in tandem or appeared to be bound to each other; they all exhibited independent, Brownian motion. We used these dynamics of the droplets to determine how the distance between two droplets should evolve over time.

We ran simulations (computer experiments) to determine the time it would take two independent droplets – localized at the same point – to separate and be resolved as distinct objects. The goal was to compare this calculated time to that at which we observed fission in our confocal microscopy experiments. The widening gap between these two times – with the simulation time for separation being less than the experimental time for fission – increased the likelihood that the droplet was a single object before fission.

The simulation parameters were the droplet diameters and their step sizes. For the simulation of the fission event in Figure 3, droplet diameters were obtained from the fluorescent micrographs in Figure 3B at $t = 0$ min for the preexisting droplet and at $t = 9.5$ min for the newly observed droplet. Both droplets have diameters larger than the resolution limit of our microscopy. Two separate sets of step sizes were assigned to the droplets. In the first, more conservative simulation, the movement of both droplets was bound by the minimum and maximum movements of the center of fluorescence of the preexisting droplet over $t = 0$ to $t = 9.5$ min. In the second simulation, the movement of one of the droplets was bound as in the first simulation, but the movement of the second droplet was bound by the minimum and maximum movements of the center of fluorescence of the newly observed droplet from $t = 9.0$ to $t = 10.0$ min. This movement of the second droplet included the separation event. In both simulations, the droplets were allowed to move independent step sizes, δ_1 and δ_2, which were random numbers between the minimum and maximum observed movements as described. Two new positions of the simulated droplets (x_1,y_1,z_1) and (x_2,y_2,z_2) were determined from $\delta_1 = (x_1^2 + y_1^2 + z_1^2)$ and $\delta_2 = (x_2^2 + y_2^2 + z_2^2)$, where six separate random numbers were generated for both sets of Cartesian co-ordinates until the above equalities matched within 1%. The subscripts in the distance equations stand for the droplet index.

At $t = 0.5$ min (the first time step of the simulation when the droplets were allowed to move), both droplets had new locations and a new distance between them, $d_{0.5} = [(x_2 \quad x_1)^2 + (y_2 \quad y_1)^2 + (z_2 \quad z_1)^2]$. If this distance was greater than the sum of the radii of the droplets plus the distance of a pixel between the droplets, the two

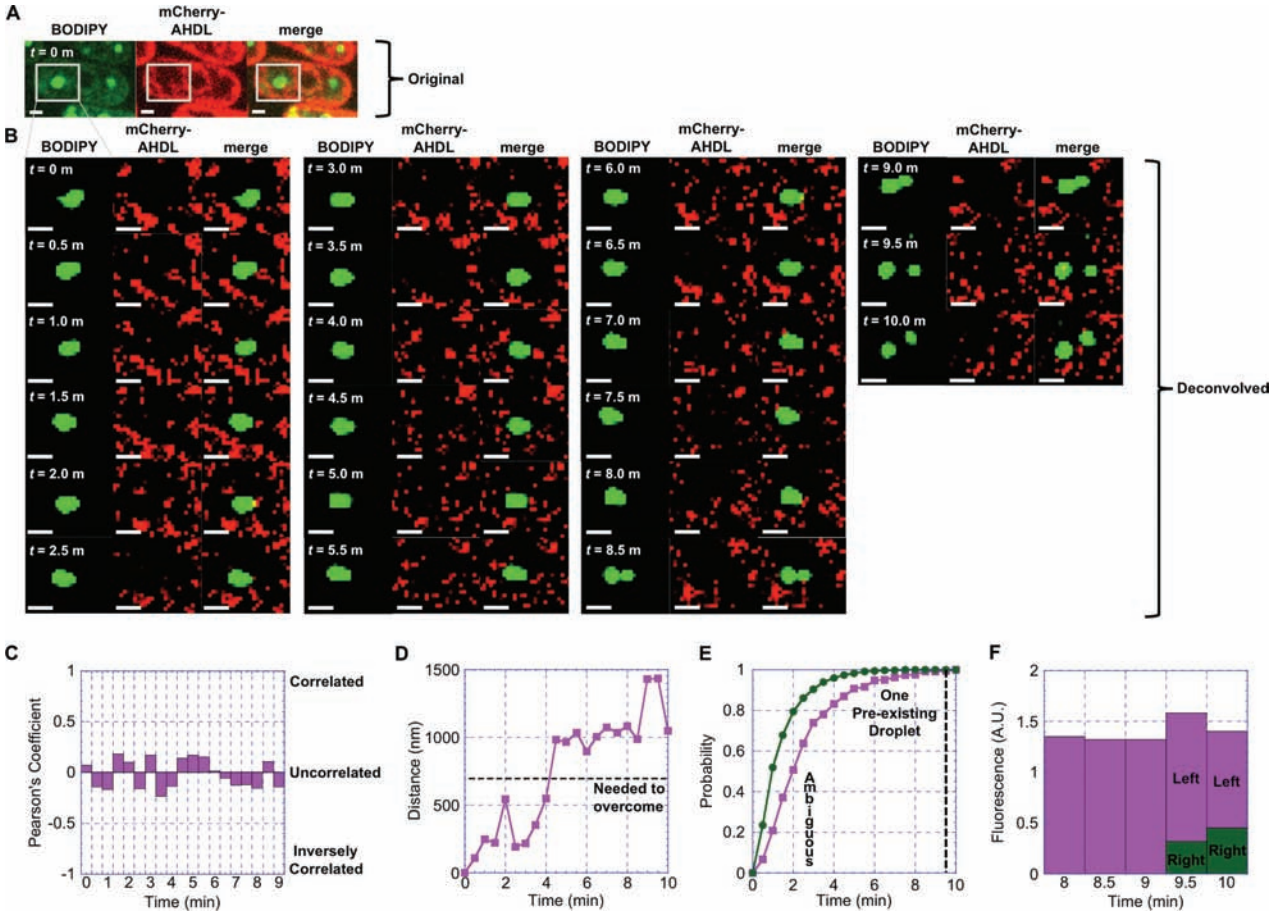

Figure 3: Fission event in G2 phase of the cell cycle. A) Original single focal plane fluorescent micrographs showing BODIPY 493/503-stained lipid droplets (left), mCherry-AHDL-labeled ER (center) and the merger of the two signals (right) in a single cell in G2 phase of the cell cycle. B) Projected maximum intensity of the BODIPY 493/503-stained lipid droplets (left), mCherry-AHDL-labeled ER (center) and the merger of the two signals (right) at specified time-points. Maximum intensities were taken from the z-stacks in which the droplets of interest were located. These images were deconvolved. C) Plot of Pearson's colocalization coefficient of the BODIPY 493/503-stained lipid droplets and mCherry-AHDL-labeled ER in the z-stacks where the preexisting and newly observed droplet were present in (B). Reported values were maximums of the calculated coefficients in each z-stack. Coefficients were not calculated for the droplets after fission was observed. D) Plot of the distance between two simulated droplets with the diameters and step sizes of the droplets obtained from (B) as described in the text. Horizontal dashed line represents the distance that the droplets must separate in order for us to observe them as two objects. E) Plot of the results of two simulations described in the text showing the high probability that the droplet in (B) is one entity and not two before $t = 9.5$ min. The two data sets represent step sizes based on the preexisting droplet (magenta) and step sizes based on both droplets (green) in (B). Vertical dashed line shows the time-point where we observed fission in (B). F) Plot of the total fluorescent intensity of the lipid droplets in (B) at the time-points just before and after fission. Data at the final two time-points are divided into the fluorescent intensity of the left (upper) and right (lower) droplets after fission. Scale bars are 1 μm.

droplets were scored as separate objects (Figure 3D). This calculation was repeated up to $t = 10.0$ min (20 steps). A sample simulation result showing the positions of the simulated droplets is provided (Figure S2).

We ran both simulations 1000 times. We recorded the number of times out of 1000 that the distance between the droplets was large enough for us to observe them as two separate objects at each of the 20 time-points. These results are presented in Figure 3E for the droplets in Figure 3A,B. From this simulation, there is less than a 0.02% chance that the fluorescent object in Figure 3B is two droplets and not a single droplet before $t = 9.5$ min.

We quantified the fluorescent intensity of the preexisting droplet *before* fission, and both the newly observed droplet and the preexisting droplet *after* fission. The sum of the intensities of the two resulting droplets compared favorably to that of the preexisting droplet at $t = 9.5$ and $t = 10.0$ min (Figure 3F). This showed that the newly observed droplet had a high probability of originating from a preexisting droplet. Also, the large fluorescent signal of

the newly observed droplet at $t = 9.5$ min was telling. The increase in the fluorescent intensity of the *de novo* droplet shown in Figure 2 can be estimated by fitting the data points from $t = 6.5$ to $t = 10.0$ min with a line where the slope of the line corresponds to an increase in 0.004 fluorescent units per minute. At this rate, the *de novo* droplet would take ~80 min to reach the fluorescent signal (0.32) of the newly observed droplet seen at $t = 9.5$ min in Figure 3B, compared to the 1 min that transpires between the first observation of a dumbbell-shaped droplet ($t = 8.5$ min) and the existence of an independent droplet ($t = 9.5$ min) (Figure 3B). Thus, it is highly unlikely that the newly observed droplet at $t = 9.5$ min in Figure 3B formed *de novo*.

To augment our time-lapse confocal microscopy experiments, we used scanning transmission electron microscopy (STEM) to obtain a higher resolution picture of lipid droplets. In particular, we wished to use an additional technique to observe lipid droplets that could be about to undergo fission.

Lipid droplets in electron micrographs have a characteristic off-white color (25). We observed several lipid droplets in cells in G2 phase (Figure 4A,B). Relevant to this work, we report droplets that were in intermediate, dumbbell-shaped states between two quasispherical droplets (Figure 4C,D). Such morphologies have also been reported in budding yeast cells (25). Again, we did not observe a signal fusion event, meaning that these intermediates have a higher probability of heading for fission than having formed from fusion.

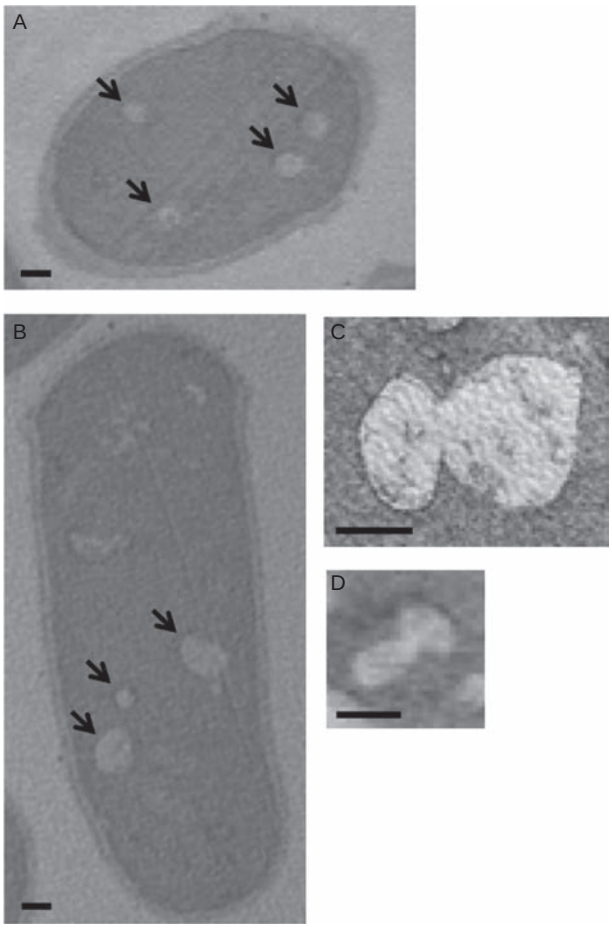

Figure 4: Electron microscopy reveals intermediate, dumbbell-shaped droplets in fission yeast cells. A and B) Electron micrographs of fission yeast cells. Lipid droplets are the off-white colored objects, the most prominent of which are indicated by arrows. C and D) Intermediate, dumbbell-shaped lipid droplets from two different cells. Scale bars are 500 nm.

Discussion

The dynamics of lipid droplets are beginning to be appreciated as a key part of cellular function (4,7,9,11,13,26–32). Here, we used time-lapse confocal microscopy to track the formation, movement and size changes of lipid droplets in the fission yeast, *S. pombe*, showing that lipid droplet number is linked to the cell cycle. The number of lipid droplets increased during G2 phase through both *de novo* formation and fission events.

In budding yeast, the major Tgl, Tgl4p, is phosphorylated and activated by Cdk1p/Cdc28p (14). This shows that a link exists between neutral lipid breakdown and the cell cycle. Because triacylglycerols are the main component of lipid droplets, Tgl4p is isolated with lipid droplet fractions, and Tgl4p-green fluorescent protein localizes to lipid droplets in budding yeast (33), a decrease in the size and/or number of lipid droplets should be observed as the budding yeast cells approached S phase. Indeed, the BODIPY 493/503 signal decreased when a constitutively active Tgl4p construct was introduced into a strain where Cdc28p was inhibited (14). However, it is not clear if the decrease in BODIPY 493/503 signal was caused by a reduction in lipid droplet number, size or both.

G2 phase in fission yeast is analogous to S phase in budding yeast in that both cells are increasing in size (34). Here, we saw an increase in the number of lipid droplets during G2 phase as fission yeast cells elongated before reaching M phase. This is the opposite of what would be expected given the findings of Kurat et al. (14). The number of lipid droplets should decrease and/or the sizes of the droplets should diminish as diacylglycerols and fatty acids would be needed as materials for expanding membranes. Tgl4p, in particular, converts triacylglycerols back into diacylglycerols where they can be incorporated into the Kennedy pathway for synthesis of phosphatidylcholine (PC) and phosphatidylethanolamine (PE) (35). Diacylglycerols can also be transformed into phosphatidic acid (PA), which can ultimately used in the traditional phospholipid synthesis pathway for the creation of phosphatidylinositol (PI), phosphatidylserine (PS), PE and PC. The lack of reduction in droplet number and size during G2 phase of the cell cycle in fission yeast suggests

that precursors for these lipids are being obtained from other locations in the cell, perhaps the ER.

It is worth speculating on the differences of the distribution of lipid droplets in cells that divide in half versus those that form a bud. It has been shown recently that a subpopulation of lipid droplets in budding yeast cells transfer into daughter cells during cell division (36). The droplets in fission yeast cells probably do not need to be actively positioned for daughter cells to acquire equal numbers of droplets. It will be interesting to determine potential differences in lipid droplet inheritance mechanisms between fission and budding yeast cells.

The number of lipid droplets remains relatively constant after G2 until the next cycle when the cells again enter G2. What factors could be responsible for the stoppage of lipid droplet number increase at the end of G2? Cdc28p (Cdk1p) must be dephosphorylated for the cell to enter M phase in budding yeast (37). Once this occurs, the primary mechanism in the production of diacylglycerols is interrupted because Cdc28p deactivates the Pah1p-encoded phosphatidate phosphatase, which is required to convert PA into diacylglycerols (38). Because the PA to diacylglycerol pathway is blocked, lipid droplet formation should also be greatly reduced if not eliminated entirely. This could be a possible checkpoint for stopping the formation of droplets as the cells leave G2 and enter M phase in yeast.

Cdc2p and Ned1p are the fission yeast orthologs of Cdc28p and Pah1p, respectively (39). Pah1p contains 15 predicted Cdk1p phosphorylation sites, although it is not clear which site is targeted by Cdc28p. Ned1p contains 19 predicted Cdk1p phosphorylation sites. Thus, Ned1p is an attractive factor that might regulate lipid droplet formation in fission yeast.

We demonstrated that formation events could be documented in yeast cells by counting the number of lipid droplets in three spatial dimensions over time. We observed instances where BODIPY 493/503 fluorescence emerged at distinct points and also cases where new droplets stably separated from preexisting droplets, both as a function of time. These results give insight into the formation mechanisms of droplets.

Several lipid droplet formation models exist (4). The most popular involves a buildup of neutral lipids in the hydrophobic regions of the ER membrane, which leads to the formation of a 'lens'. When the lens reaches a critical size, it leaves the ER, surrounded by phospholipids from the ER membrane. The fluorescence increase and the localization of the lipid droplet in Figure 2 agree with this model. However, higher resolution techniques such as photoactivation localization microscopy and clever electron microscopy experiments will probably have to be utilized to test the mechanistic details of droplet biogenesis.

We observed five lipid droplet fission events during G2 phase of the cell cycle. The formation of droplets by this mechanism has not, to our knowledge, been seen up until this point (10). The mechanisms of droplet fission are unknown but factors involved in bending bilayer membranes would be a starting point. A recent proteomic study on lipid droplets purified from budding yeast identified the BAR (Bin-amphiphysin-Rvs167) domain-containing protein GVP36p (YIL041W) in the lipid droplet fraction (40). Mug64p is the fission yeast ortholog of this factor. However, factors that could cause organelle fission may not be easily identifiable (41). Much work remains to determine the force generation required for fission.

The synthesis of neutral lipids has been hypothesized to occur on or in the droplets themselves (9). Triacylglycerol synthesis was documented in fractions containing droplets that were isolated from cells (42,43). Here, we showed that changes in the fluorescent intensity of BODIPY 493/503-labeled droplets over time were a key signature of all droplets in fission yeast cells. Smaller droplets have larger relative changes in fluorescence compared to larger droplets. This agrees with postulates that smaller droplets are more favorable for lipolysis than larger droplets because the former have greater exposed surface area over volume than the latter (44). As small droplets predominate in fission yeast, they may be the preferred source for needed materials that result from the breakdown of neutral lipids.

Materials and Methods

Fission yeast cells were prepared for visualization by confocal microscopy as follows. Cells having mCherry-AHDL integrated into their leu1+ locus (gift from S. Oliferenko, National University of Singapore (18)) were cultured in YE5S media (#2011, Sunrise Science Products) to late log phase: $OD_{595} < 0.5$ at 30 C. The total volume of the cell culture was 20 mL. The cells were then pelleted at 850 × ***g*** in a swinging bucket centrifuge, and all but 1 mL of the YE5S was removed. The lipid droplets were resuspended in this volume and stained with BODIPY 493/503 (#D3922, Invitrogen).

We followed established methods for visualizing fluorescent objects in fission yeast cells using time-lapse confocal microscopy (17,45,46). Five to ten microliters of the above reserved cells was added to the top of a pad made of EMM5S (#2005, Sunrise Science Products) and 25% gelatin that was fixed on a glass slide. The pad reduced drift during time-lapse experiments. A coverslip was placed over the sample, extra YE5S media was added to fill the chamber and the chamber was subsequently sealed. All results presented from confocal microscopy experiments were from a single sample, thus the conditions were identical for all cells.

We recorded the dynamic properties of BODIPY 493/503-stained lipid droplets in live cells using a spinning-disk confocal system (UltraView RS, Perkin Elmer) that had recently been used to acquire highly accurate measurements of fluorescent intensity for other cellular factors (17). We used a 60×/1.4 NA objective with an additional 1.5× magnification resulting in 133 nm/pixel resolution in the *x*, *y* plane and 360 nm in the *z* plane. These resolutions are acceptable by the laws of Abbe (24). Yeast cells were spanned by enough slices to avoid undersampling but not too many to skew toward oversampling. Time between exposures was 100 milliseconds. Digital images were processed with ImageJ software and were deconvolved with AutoQuant X software for quantitative analysis. Ten

iterations of 3D deconvolution were performed using a fixed theoretical point spread function.

Simulations were written in c++ using the Xcode compiler and were run on a MacBook Pro. Each simulation took about 5 seconds for completion.

Samples for electron microscopy were prepared according to the methods described by Wright (47). Briefly, sample were fixed in PIPES buffered glutaraldehyde, followed by postfixation in potassium permanganate then *en bloc* stained with uranyl acetate before embedding in Spurr's epoxy. Thin sections (<100 nm) were cut on a Leica EM UC7 ultramicrotome and examined with a Zeiss Auriga operating in STEM mode.

Acknowledgments

The authors thank Rajesh Arasada (Yale University) and Chad McCormick (Yale University) for assistance with microscopy and general yeast troubleshooting, Thomas D. Pollard (Yale University) for allowing the use of his confocal microscope, Richard McIntosh and members of his laboratory (University of Colorado) for sharing his EM images, Joel Goodman (UT Southwestern) for EM troubleshooting and Alex Meyers (University of Tennessee) for valuable input for the *Discussion* section.

Supporting Information

Additional Supporting Information may be found in the online version of this article:

Figure S1: Technique for obtaining the volume of small lipid droplets from fluorescent intensities. Plot of the fluorescent intensity of 20 large droplets as a function of their volumes. Volumes were obtained through the equation, $V = 4\pi/3(d/2)^2$, where d is the measured diameter of a droplet. Inset is a fluorescent micrograph of a BODIPY 493/503-stained lipid droplet. Arrows indicate the diameter of the droplet. This droplet has a calculated diameter of ~800 nm. Scale bar is 1 μm.

Figure S2: Simulations of lipid droplet fission. Spheres represent the droplets in the simulation described in the text. The results of which are shown in Figure 3D. Note the overlap of the two droplets before t = 4.5 min.

Movie 1: *De novo* lipid droplet formation event in G2 phase of the cell cycle. Movie shows the formation event in Figure 2B of the text (spans 10 min).

Movie 2: Fission event in G2 phase of the cell cycle. Movie shows the fission event in Figure 3B of the text (spans 10 min).

Please note: Wiley-Blackwell are not responsible for the content or functionality of any supporting materials supplied by the authors. Any queries (other than missing material) should be directed to the corresponding author for the article.

References

1. Athenstaedt K, Zweytick D, Jandrositz A, Kohlwein SD, Daum G. Identification and characterization of major lipid particle proteins of the yeast *Saccharomyces cerevisiae*. J Bacteriol 1999;181:6441–6448.
2. Zweytick D, Athenstaedt K, Daum G. Intracellular lipid particles of eukaryotic cells. Biochim Biophys Acta 2000;1469:101–120.
3. Ploegh HL. A lipid-based model for the creation of an escape hatch from the endoplasmic reticulum. Nature 2007;448:435–438.
4. Walther TC, Farese RV Jr. The life of lipid droplets. Biochim Biophys Acta 2009;1791:459–466.
5. Zanghellini J, Wodlei F, von Grunberg HH. Phospholipid demixing and the birth of a lipid droplet. J Theor Biol 2010;264:952–961.
6. Ohsaki Y, Cheng J, Suzuki M, Shinohara Y, Fujita A, Fujimoto T. Biogenesis of cytoplasmic lipid droplets: from the lipid ester globule in the membrane to the visible structure. Biochim Biophys Acta 2009;1791:399–407.
7. Roingeard P, Depla M. The birth and life of lipid droplets: learning from the hepatitis C virus. Biol Cell 2011;103:223–231.
8. Robenek H, Hofnagel O, Buers I, Robenek MJ, Troyer D, Severs NJ. Adipophilin-enriched domains in the ER membrane are sites of lipid droplet biogenesis. J Cell Sci 2006;119:4215–4224.
9. Farese RV Jr. Walther TC. Lipid droplets finally get a little R-E-S-P-E-C-T. Cell 2009;139:855–860.
10. Thiele C, Spandl J. Cell biology of lipid droplets. Curr Opin Cell Biol 2008;20:378–385.
11. Goodman JM. The gregarious lipid droplet. J Biol Chem 2008;283: 28005–28009.
12. Zehmer JK, Huang Y, Peng G, Pu J, Anderson RGW, Liu P. A role for lipid droplets in inter-membrane lipid traffic. Proteomics 2009;9:914–921.
13. Murphy S, Martin S, Parton RG. Lipid droplet-organelle interactions; sharing the fats. Biochim Biophys Acta 2009;1791:441–447.
14. Kurat CF, Wolinski H, Petschnigg J, Kaluarachchi S, Andrews B, Natter K, Kohlwein SD. Cdk1/Cdc28-dependent activation of the major triacylglycerol lipase tgl4 in yeast links lipolysis to cell-cycle progression. Mol Cell 2009;33:53–63.
15. Gocze PM, Freeman DA. Factors underlying the variability of lipid droplet fluorescence in MA-10 Leydig tumor cells. Cytometry 1994;17:151–158.
16. Kwok ACM, Wong JTY. Lipid biosynthesis and its coordination with cell cycle progression. Plant Cell Physiol 2005;46:1973–1986.
17. Wu JQ, Pollard TD. Counting cytokinesis proteins globally and locally in fission yeast. Science 2005;310:310–314.
18. Zhang D, Vjestica A, Oliferenko S. The cortical ER network limits the permissive zone for actomyosin ring assembly. Curr Biol 2010;20:1029–1034.
19. Listenberger LL, Brown DA. Fluorescent detection of lipid droplets and associated proteins. Curr Protoc Cell Biol 2007;24.2.1–24.2.11.
20. Otsu N. A threshold selection method from gray-level histograms. IEEE Trans Sys Man Cyber 1979;9:62–66.
21. Mandal SK, Lequeux N, Rotenberg B, Tramier M, Fattaccioli J, Bibette J, Dubertret B. Encapsulation of magnetic and fluorescent nanoparticles in emulsion droplets. Langmuir 2005;21:4175–4179.
22. Chaikin PM, Lubensky TC. Principles of Condensed Matter Physics. England: Cambridge University Press; 2000.
23. Sabatinos SA, Forsburg SL. Measuring DNA content by flow cytometry in fission yeast. Methods Mol Biol 2009;521:449–461.
24. Bolte S, Cordelieres FP. A guided tour into sub cellular colocalization analysis in light microscopy. J Micros 2006;224:213–232.
25. Binns D, Januszewski T, Chen Y, Hill J, Markin VS, Zhao Y, Gilpin C, Chapman KD, Anderson RGW, Goodman JM. An intimate collaboration between peroxisomes and lipid bodies. J Cell Biol 2006;173:719–731.
26. Martin S, Parton RG. Lipid droplets: a unified view of a dynamic organelle. Nat Rev Mol Cell Biol 2006;7:373–378.
27. Welte MA, Cermelli S, Griner J, Viera A, Guo Y, Kim DH, Ginhart JG, Gross SP. Regulation of lipid-droplet transport by the perilipin homolog LSD2. Curr Biol 2005;15:1266–1275.
28. Kalantari F, Bergeron JJM, Nilsson T. Biogenesis of lipid droplets – how cells get fatter. Mol Membr Biol 2010;27:462–468.
29. Beller M, Thiel K, Jackle H. Lipid droplets: a dynamic organelle moves into focus. FEBS Lett 2010;584:2176–2182.
30. Somwar R, Roberts CT, Varlamov O. Live-cell imaging demonstrates rapid cargo exchange between lipid droplets in adipocytes. FEBS Lett 2011;585:1946–1950.
31. Welte MA. Fat on the move: intracellular motion of lipid droplets. Biochem Soc Trans 2009;37:991–996.
32. Digel M, Ehehalt R, Fullekrug J. Lipid droplets lighting up: insights from live microscopy. FEBS Lett 2010;584:2168–2175.
33. Athenstaedt K, Daum G. Tgl4p and Tgl5p, two triacylglycerol lipases of the yeast *Saccharomyces cerevisiae*, are localized to lipid particles. J Biol Chem 2005;280:37301–37309.
34. Forsburg SL, Nurse P. Cell cycle regulation in the yeasts *Saccharomyces cerevisiae* and *Schizosaccharomyces pombe*. Annu Rev Cell Biol 1991;7:227–256.

35. Kresge N, Simoni RD, Hill RL. The Kennedy pathway for phospholipid synthesis: the work of Eugene Kennedy. J Biol Chem 2005;280:e22–e24.
36. Wolinksi H, Kolb D, Hermann S, Koning RI, Kohlwein SD. J Cell Sci 2011;124:3894–3904.
37. Nurse P. Universal control mechanism regulating onset of M-phase. Nature 1990;459:857–860.
38. O'Hara L, Han GS, Peak-Chew S, Grimsey N, Carman GM, Siniossoglou S. Control of phospholipid synthesis by phosphorylation of the yeast lipin Pah1/Smp2p Mg2+-dependent phosphatidate phosphatase. J Biol Chem 2006;281:34537–34548.
39. Penkett CJ, Morris JA, Wood V, Bahler J. YOGY: a web-based, integrated database to retrieve protein orthologs and associated gene ontology terms. Nucleic Acids Res 2006;34:W330–W334.
40. Grillitsch K, Connerth M, Kofeler H, Arrey TN, Rietschel B, Wagner B, Karas M, Daum G. Lipid particles/droplets of the yeast *Saccharomyces cerevisiae* revisited: lipidome meets proteome. Biochim Biophys Acta 2011;1811:1165–1176.
41. Friedman JR, Lackner LL, West M, DiBenedetto JR, Nunnari J, Voeltz GK. ER tubules mark sites of mitochondrial division. Science 2011;334:358–362.
42. Fujimoto Y, Itabe H, Kinoshita T, Homma K, Onoduka J, Mori M, Yamaguchi S, Makita M, Higashi Y, Yamashita A, Takano T. Involvement of ACSL in local synthesis of neutral lipids in cytoplasmic lipid droplets in human hepatocyte HuH7. J Lipid Res 2007;48:1280–1292.
43. Kuerschner L, Moessinger C, Thiele C. Imaging of lipid biosynthesis: how a neutral lipid enters lipid droplets. Traffic 2008;9:338–352.
44. Nishino N, Tamori Y, Tateya S, Kawaguchi T, Shibakusa T, Mizunoya W, Inoue K, Kitazawa R, Kitazawa S, Matsuki Y, Hiramatsu R, Masubuchi S, Omachi A, Kimura K, Saito M, et al. FSP27 contributes to efficient energy storage in murine white adipocytes by promoting the formation of unilocular lipid droplets. J Clin Invest 2008;118:2808–2821.
45. Sirotkin V, Beltzner CC, Marchand JB, Pollard TD. Interactions of WASp, myosin-I, and verprolin with Arp2/3 complex during actin patch assembly in fission yeast. J Cell Biol 2005;170:637–648.
46. Wu JQ, Sirotkin V, Kovar DR, Lord M, Beltzner CC, Kuhn JK, Pollard TD. Assembly of the cytokinetic contractile ring from a broad band of nodes in fission yeast. J Cell Biol 2006;174:391–402.
47. Wright R. Transmission electron microscopy of yeast. Microsc Res Tech 2000;51:496–510.